

# A general optical flow based terrain-following strategy for a VTOL UAV using multiple views

Bruno Herisse, Sophie Oustrieres, Tarek Hamel, Robert Mahony, Francois-Xavier Russotto

**Abstract**—This paper presents a general approach for terrain following (including obstacle avoidance) of a vertical take-off and landing vehicle (VTOL) using multiple observation points. The VTOL vehicle is assumed to be a rigid body, equipped with a minimum sensor suite (camera, IMU and barometric altimeter), manoeuvring over a textured rough terrain made of a concatenation of planar surfaces. Assuming that the forward velocity is separately regulated to a desired non-zero value, the proposed control approach ensures terrain following and guarantees the vehicle does not collide with obstacles during the task. The proposed control acquires an optical flow from multiple spatially separate observation points, typically obtained via multiple cameras or non collinear directions in a unique camera. The proposed control algorithm has been tested extensively in simulation and then implemented on a quadrotor UAV to demonstrate the performance of the closed loop system.

## I. INTRODUCTION

The past decade has seen an explosive growth of interest in Unmanned Aerial Vehicles (UAVs) [1]. Such vehicles have strong commercial potential in automatic or remote surveillance applications such as monitoring traffic congestion, regular inspection of infrastructure such as bridges, dam walls, power lines, forest fire or investigation of hazardous environments, to name only a few of the possibilities. There are also many indoors applications such as inspection of infrastructures in mines or large buildings, and search and rescue in dangerous enclosed environments. Autonomous flight in confined or cluttered environments requires cheap and robust sensor systems that are light enough to be carried by the vehicle and which provide sufficient information for a high manoeuvrability. Historically, payload constraints have severely limited autonomy of a range of micro aerial vehicles. The small size, highly coupled dynamics and ‘low cost’ implementation of such systems provide an ideal testing ground for sophisticated non-linear control techniques. A key issue arising is the difficulty of navigation through cluttered environments and close to obstructions (obstacle avoidance, take-off and landing). Since optical flow provides proximity information [2], this cue can be used to navigate around obstacles without collision [3], [4], [5], [6]. When optical flow is combined with the forward velocity, several authors have investigated the height regulation of the UAVs above the terrain using linear control techniques [7], [8], [9]. The

potential complexity of the environment makes us understand that multiple directions of observation are necessary to ensure collision free navigation. More recently other works have been carried out using the measurement of different direction of the optical flow for reflexive obstacle avoidance [10], [11]. In [12] a biomimetic navigation in corridors that combines left and right optical flows in a control scheme with application to hovercraft was considered. In [13] the measurement of two non-collinear directions are combined to ensure a wide range of terrain following including slopes. Based on our prior work [14], this paper provides a general approach for terrain following in 3-D space using multiple directions of observation. The controller ensures obstacle avoidance of an UAV capable of quasi stationary flight. We consider control of the translational dynamics of the vehicle and in particular focus on regulation of the forward optical flow along with a guarantee that the vehicle will not collide with the surrounding environment. A ‘high gain’ controller is used to stabilise the orientation dynamics; this approach is classically known in aeronautics as guidance and control (or hierarchical control) [15]. The image feature considered is the average optical flow obtained from the measurement of the optical flow of a textured obstacle in the inertial frame using additional information provided by an embedded IMU for *derotation* of the flow. The terrain is assumed to be made of a concatenation of planar surfaces. Robustness analysis of the control scheme is performed to ensure obstacle avoidance and to prove global practical stability of the closed-loop system for terrain following. The control algorithm has been tested extensively in simulation and then implemented on a quadrotor UAV developed by the CEA (French Atomic Energy Commission). Experiments of the proposed approach demonstrate efficiency and performance for terrain following. The body of the paper consists of five sections followed by a conclusion. Section II presents the fundamental equations of motion for the quadrotor UAV. Section III presents the proposed control strategies for terrain following and Section IV assesses the robustness of the controller. Section V describes simulation results and Section VI presents the experimental results obtained on the quadrotor vehicle.

## II. UAV DYNAMIC MODEL AND TIME SCALE SEPARATION

The VTOL UAV is represented by a rigid body, of mass  $m$  and of tensor of inertia  $\mathbf{I}$ , with external forces due to gravity and forces and torques applied by rotors. To describe the motion of the UAV, two reference frames are introduced: an inertial reference frame  $\mathcal{I}$  associated with the vector basis  $[e_1, e_2, e_3]$  and a body-fixed frame  $\mathcal{B}$  attached to the

B. Herisse, S. Oustrieres and F.-X. Russotto are with CEA/List, Fontenay-Aux-Roses, France `firstname.lastname@cea.fr`

T. Hamel is with I3S, UNSA - CNRS, Sophia Antipolis, France `thamel@i3s.unice.fr`

R. Mahony is with Dep. of Eng., Australian Nat. Univ., ACT, 0200 Australia `Robert.Mahony@anu.edu.au`

UAV at the center of mass and associated with the vector basis  $[e_1^b, e_2^b, e_3^b]$ . The position and the linear velocity of the UAV in  $\mathcal{I}$  are respectively denoted  $\xi = (x, y, z)^T$  and  $v = (\dot{x}, \dot{y}, \dot{z})^T$ . The orientation of the UAV is given by the orientation matrix  $R \in SO(3)$  from  $\mathcal{B}$  to  $\mathcal{I}$ , usually parameterized by Euler's angles  $\psi, \theta, \phi$  (yaw, pitch, roll). Finally, let  $\Omega = (\Omega_1, \Omega_2, \Omega_3)^T$  be the angular velocity of the UAV defined in  $\mathcal{B}$ .

A translational force  $F$  and a control torque  $\Gamma$  are applied to the UAV. The translational force  $F$  combines thrust, lift, drag and gravity components. For a miniature VTOL UAV in quasi-stationary flight one can reasonably assume that the aerodynamic forces are always in direction  $e_3^b$ , since the thrust force predominates over other components [16]. The gravitational force can be separated from other forces and the dynamics of the VTOL UAV can be written as:

$$\dot{\xi} = v \quad (1)$$

$$m\dot{v} = -TRe_3 + mge_3 \quad (2)$$

$$\dot{R} = R\Omega_\times, \quad (3)$$

$$\mathbf{I}\dot{\Omega} = -\Omega \times \mathbf{I}\Omega + \Gamma, \quad (4)$$

In the above notation,  $g$  is the acceleration due to gravity, and  $T$  a scalar input termed the thrust or heave, applied in direction  $e_3^b = Re_3$  where  $e_3$  is the third-axis unit vector  $(0, 0, 1)$ . The matrix  $\Omega_\times$  denotes the skew-symmetric matrix associated to the vector product  $\Omega_\times x := \Omega \times x$  for any  $x$ .

### III. TERRAIN FOLLOWING STRATEGY

This section aims at presenting a general approach based on a previous work [14] for terrain following. The observed surface in a given direction is assumed to be locally planar and cameras are assumed to be attached to the center of mass so that the focal point of cameras coincide with the origin of the body-fixed frame.

#### A. Optical flow cue

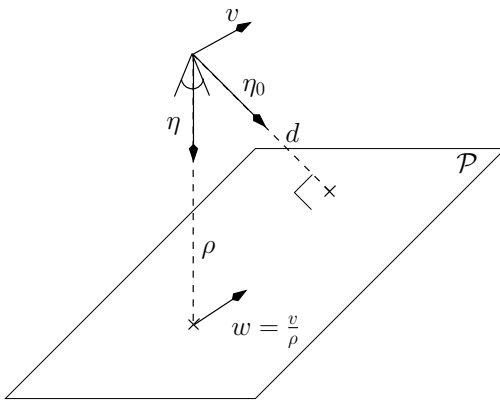


Fig. 1: Average optical flow

The optical flow can be computed using a range of algorithms (correlation-based technique, features-based approaches, differential techniques, etc) [17]. Note that due

to the rotational ego-motion of the camera, the optical flow involves the angular velocity as well as the linear velocity [2]. Let  $\eta \in \mathcal{I}$  denote the unit vector in the direction of observation and  $\eta_0 \in \mathcal{I}$  the unit normal to the target plane (see Figure 1). We define an inertial average optical flow from the integral of all observed optical flow around the direction of observation  $\eta$  corrected for rotational angular velocity

$$w = -(R_t \Lambda^{-1} R_t^T) R \iint_{\mathcal{W}^2} (\dot{p} + \Omega \times p) dp \quad (5)$$

where  $\dot{p}$  is the derivative of an image point  $p$  observed by a spherical camera,  $\mathcal{W}^2$  is the aperture around  $\eta$ ,  $\Lambda$  is a diagonal matrix depending on the aperture and  $R_t$  is the orientation matrix from a frame of reference with  $\eta$  in the z-axis to the inertial frame  $\mathcal{I}$  (see details in [14]). We make the assumption that an observed surface is stationary and planar or locally planar. The distance of the camera to that target plane is denoted  $d$ . Then the average optical flow  $v/d$  can be obtained when the observed direction is  $\eta_0$ . If the normal to the target plane  $\eta_0$  is unknown, the optical flow  $w$  obtained from the observation in a different direction  $\eta$  can be written:

$$w = M(\eta_0, \eta) \frac{v}{\rho} \quad (6)$$

$$= M(\eta_0, \eta) \frac{v}{d} \cos(\langle \eta_0, \eta \rangle) \quad (7)$$

where  $M$  is a full-rank matrix equal to identity when  $\eta = \eta_0$  (if  $\eta$  and  $\eta_0$  are non-collinear  $M \neq I_3$ ). Since  $\eta_0$  is, in practice, an unknown direction, it is not possible to invert for  $M(\eta_0, \eta)$  to estimate  $v/\rho$  from  $w$ . The approach taken is to develop the control based on the assumption  $M(\eta_0, \eta) = I_3$ , hence  $w = v/\rho$ , and then analyse the robustness of the closed loop system with respect to modelling errors.

For the remainder of Section III we assume

$$w = \frac{v}{\rho} \quad (8)$$

#### B. Terrain following by forward optical flow conservation

In this section a control design ensuring terrain, wall or relief following is proposed. The control problem considered is the stabilisation of a *pseudo distance*  $d$  around a set point  $d^*$  while ensuring non collision. The measurements of the optical flow in  $n$  non-collinear directions are considered. Let  $\eta_i$  be the  $i$ th direction of observation and let  $w_i$  be its associated average optical flow. A non-linear controller depending on measurable variables  $w_i$  is developed for the translational dynamics (2). The full vectorial term  $TRe_3$  will be considered as control input for these dynamics. We will assign its desired value  $u \equiv (TRe_3)^d = T^d R^d e_3$ . Assuming that actuator dynamics can be neglected, the value  $T^d$  is considered to be instantaneously reached by  $T$ . For the orientation dynamics of (3)-(4), a high gain controller is used to ensure that the orientation  $R$  of the UAV converges to the desired orientation  $R^d$ . The resulting control problem is simplified to

$$\dot{\xi} = v, m\dot{v} = -u + mge_3 \quad (9)$$

Thus, we consider only control of the translational dynamics (9) with a direct control input  $u$ . This common approach is used in practice and may be justified theoretically using singular perturbation theory [18].

Define  $\beta$  as the unit vector collinear to the sum of all the directions of observation  $\eta_i$  weighted by the associated optical flow  $w_i$ . That is

$$\beta = \frac{\sum_{i=1}^n \|w_i\| \eta_i}{\|(\sum_{i=1}^n \|w_i\| \eta_i)\|} = \frac{\sum_{i=1}^n \eta_i / \rho_i}{\|(\sum_{i=1}^n \eta_i / \rho_i)\|} \quad (10)$$

Note that a direction for which an obstacle has larger average optical flow and consequently is closer to the camera, has a higher weight than another. We also define the following average optical flow

$$w_\beta = \sum_{i=1}^n (\eta_i^\top \beta) w_i \quad (11)$$

It is not immediately clear what represents  $w_\beta$ . Developing  $w_\beta$  recalling (8) and (10), we obtain

$$w_\beta = v \left( \sum_{i=1}^n \frac{\eta_i^\top}{\rho_i} \right) \beta = v \left( \left\| \sum_{i=1}^n \eta_i / \rho_i \right\| \beta^\top \right) \beta = \frac{v}{d}$$

where  $d = \|\sum_{i=1}^n \eta_i / \rho_i\|^{-1}$  is termed the *pseudo distance*.  $w_\beta$  may be interpreted as the average optical flow measured in direction  $\beta$  from a single camera observing a virtual obstacle with  $d$  the distance between the camera and the obstacle. We define two components of  $w_\beta$  that we term the normal optical flow ( $w_\beta^\perp$ ) and the forward optical flow ( $w_\beta^\parallel$ ) as follows:

$$w_\beta^\perp = \langle \beta, w_\beta \rangle \quad (12)$$

$$w_\beta^\parallel = \pi_\beta w_\beta \quad (13)$$

where  $\pi_\beta = (I_3 - \beta\beta^\top)$  is a semi-definite projection matrix.

The control strategy proposed in this paper consists in applying a control input  $u$  that allows regulation of the forward optical flow to a constant  $\omega^*$  while preserving the norm of the forward velocity. Since the norm of the desired forward velocity  $v^r$  is assumed to be constant ( $\|v^r\| = v^*$ ), only the orientation of the vector  $v^r$  can vary over time due to variation of  $\beta$  ( $v^r = \pi_\beta v^r$ ). We define  $\Omega_v$  as the angular velocity of the reference velocity  $v^r$ , thus,  $dv_r/dt = \Omega_v \times v^r$ .

With the above objective, the controller is divided in two parts. The first controller ensures regulation of  $(v - v^r)$  in the plane normal to  $\beta$ :

$$u^\parallel = k_v (v^\parallel - v^r) - m\pi_\beta (\Omega_v \times v) + mg\pi_\beta e_3 \quad (14)$$

where  $v^\parallel = \pi_\beta v$  and  $k_v$  is a positive parameter.

The second controller, acting in the direction  $\beta$ , aims at regulating the tangential (or forward) optical flow to a constant  $\omega^*$  with the normal flow  $w_\beta^\perp$  is used as an additional damping term:

$$u^\perp = k_D w_\beta^\perp + k_P \left( \|w_\beta^\parallel\| - \omega^* \right) - m \langle \Omega_v \times v - ge_3, \beta \rangle \quad (15)$$

where  $k_D$  and  $k_P$  are positive parameters. Since the forward velocity must be close to the set point  $v^r$  at any time to insure good detection of the optical flow, the control gain  $k_v$  must be chosen such that  $k_v \gg k_P, k_D$ . The term  $\Omega_v \times v$  is used to compensate for variations of  $v^r$  (and  $\beta$ ). Note that if the regulation is achieved,  $\|w_\beta^\parallel\| \equiv \omega^*$  is a function of  $v^*$ .

This means that if  $\|w_\beta^\parallel\|$  converges around  $\omega^*$ ,  $d$  converges around  $d^* = v^*/\omega^*$ .

Introducing both controllers (14-15) in the translational dynamics (9), it yields:

$$m \frac{d}{dt} (v^\parallel - v^r) = -k_v (v^\parallel - v^r) \quad (16)$$

$$m \frac{d}{dt} v^\perp = -k_D w_\beta^\perp - k_P \left( \|w_\beta^\parallel\| - \omega^* \right) \quad (17)$$

Note that the stability of system (16) is obvious. The stability proof of system (17) is however more complex. It is provided in our previous work [14] in the situation where only one direction of observation is used. Before introducing robustness analysis of the proposed control scheme in the situation where multiple measurements are used, two illustrative examples are considered.

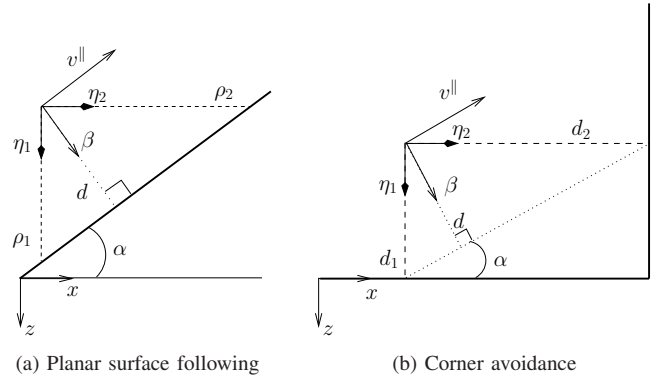


Fig. 2

1) *The case of the planar surface:* The control problem is to follow a plane using two directions of observation. Assume that the two directions  $\eta_1$  and  $\eta_2$  are perpendicular (see Figure 2a) and the desired forward velocity is in the plane defined by these two directions (2-D motion).

In that case, from equations (10), (12) and (13), it is straightforward to show that:

$$\beta = (\sin \alpha, \cos \alpha)^\top \quad (18)$$

$$w_\beta^\perp = \frac{\langle \beta, v \rangle}{d} = \frac{v^\perp}{d} = -\frac{\dot{d}}{d} \quad (19)$$

$$w_\beta^\parallel = \frac{\pi_\beta v}{d} = \frac{v^\parallel}{d} \quad (20)$$

where  $v^\perp = \langle \beta, v \rangle$ . Note that  $\beta = \eta_0$ , the normal to the observed plane, hence  $v^\perp = -\dot{d}$ .

Recall the dynamics of the component of (9) in the

direction  $\beta$  and the control law (15), it yields:

$$m\ddot{d} = -k_D \frac{\dot{d}}{d} + k_P \left( \frac{\|v^\parallel\|}{d} - \omega^* \right) \quad (21)$$

When the regulation of the forward velocity  $v^\parallel$  to  $v^r$  is achieved, one obtains the equation studied in the previous work [14]. It has been shown that for all initial conditions such that  $d(0) = d_0 > 0$ , the closed-loop trajectory exists for all time and satisfies  $d(t) > 0, \forall t$ . Moreover,  $d(t)$  converges asymptotically to  $d^*$ . Note that contrary to the case where one direction ( $n = 1$ ) is used, the controller is stable for any slope  $\alpha$  between 0 and  $\pi/2$  and for any positive gains  $k_P$  and  $k_D$ . The robustness of the approach has been increased by adding a second direction of observation.

2) *Corner avoidance*: The control problem is to avoid the corner of a room or a wall that appears in the direction of motion. Assume that the two directions  $\eta_1$  and  $\eta_2$  are perpendicular (see Figure 2b) and the desired forward velocity is in the plane defined by these two directions (2-D motion).

In that case, from equations (10), (12) and (13), it is straightforward to show that:

$$\beta = \left( \frac{d_1}{\sqrt{d_1^2 + d_2^2}}, \frac{d_2}{\sqrt{d_1^2 + d_2^2}} \right)^\top = (\sin \alpha, \cos \alpha)^\top \quad (22)$$

$$w_\beta^\perp = \frac{\langle \beta, v \rangle}{d} = \frac{v^\perp}{d} \quad (23)$$

$$w_\beta^\parallel = \frac{\pi_\beta v}{d} = \frac{v^\parallel}{d} \quad (24)$$

where  $\tan \alpha = d_1/d_2$  and  $d = d_1 d_2 / \sqrt{d_1^2 + d_2^2}$ . Figure 3 represents the desired trajectory  $d = d^*$ . Note that the function  $d$  is defined with respect to a virtual plane that itself depends on the local geometry and position of the vehicle. As a consequence, the *pseudo distance*  $d$  is a highly non-linear function of position. In particular, unlike actual distance such as was considered in case III-B.1, the gradient of  $d$  is not colinear with  $\beta$ . Straightforward calculations yield

$$\begin{aligned} \nabla d &= - \left( \left( \frac{d_1}{\sqrt{d_1^2 + d_2^2}} \right)^3, \left( \frac{d_2}{\sqrt{d_1^2 + d_2^2}} \right)^3 \right)^\top \\ &= -(\sin(\alpha)^3, \cos(\alpha)^3)^\top \end{aligned}$$

while  $\beta$  is given by (22). Recall the dynamics of the component of (9) in the direction  $\beta$  and the control law (15), it yields:

$$m\dot{v}^\perp = m \frac{dv^\perp}{dt} = -k_D \frac{v^\perp}{d} - k_P \left( \frac{\|v^\parallel\|}{d} - \omega^* \right) \quad (25)$$

When the regulation of the forward velocity  $v^\parallel$  to  $v^r$  is achieved, one obtains a similar equation as the previous case (21). Note however that  $v^\perp \neq -\dot{d}$  and the stability is not guaranteed a priori. One can write the direction of  $\nabla d$  as  $(-\sin \alpha', -\cos \alpha')$  where  $\tan \alpha' = \tan(\alpha)^3$ . Note that  $\tan(\alpha - \alpha') < 0.36$  for all  $\alpha$  such that  $0 \leq \alpha \leq \pi/2$ .

This ensures that the direction of the gradient of  $d$  with respect to  $x$  and  $z$  remains close to the direction  $-\beta$ . That is, the controller acts in a direction close to the opposite of the gradient of  $d$ . Let  $v_d$  denote the velocity of the UAV in the opposite direction of the gradient of  $d$ :  $v_d = -\langle v, \nabla d \rangle / \|\nabla d\| = -\dot{d} / \|\nabla d\|$ . The dynamics of the system in this direction can be written as follows:

$$m\dot{v}_d = m \frac{dv_d}{dt} = k_P \omega^* \gamma \left( 1 - \frac{d^*}{d} \chi \right) - k_D \frac{v_d}{d} \quad (26)$$

where  $\gamma = \cos(\alpha - \alpha')$  and  $\chi = (1 + \tan(\alpha - \alpha')k_D/k_P)$ . The gains  $k_P$  and  $k_D$  must be chosen such that  $\chi$  is positive and bounded.

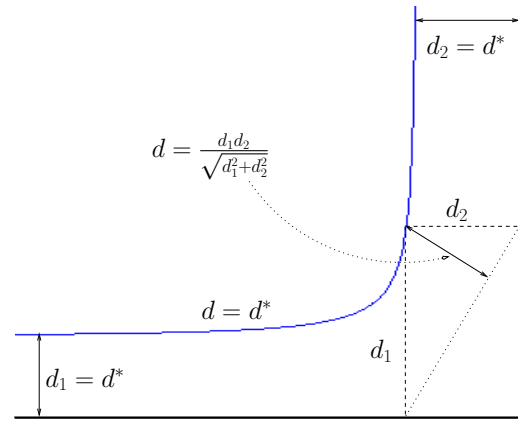


Fig. 3: The desired trajectory  $d = d^*$

*Remark 3.1*: Only a 2-D control approach is considered in these two examples. However, the general approach can also be used for full 3-D motion by adding additional cameras, for example, on the leftside or rightside of the UAV. In this case the dynamics (16) and (17) are still valid, although, the special cases III-B.1 and III-B.2 considered above only hold in very specific geometries. It is beyond the scope of this paper to analyse the 3-D case in detail. We believe, however, that the results for 3-D will be qualitatively the same as for the results obtained in this paper.  $\triangle$

#### IV. ROBUSTNESS TO NOISE AND UNCERTAINTIES

In this section we consider the robustness of the previous controller in case where  $v^\perp \neq -\dot{d}$ . Analogously to the analysis of Section III-B.2, it can be shown in the general case that the dynamics of the system in the opposite direction of the gradient of  $d$  can be written:

$$m\dot{v}_d = m \frac{dv_d}{dt} = k_P \omega^* \gamma(t) \left( 1 - \frac{d^*}{d} \chi(t) \right) - k_D \delta(t) \frac{v_d}{d} \quad (27)$$

where  $v_d = -\dot{d} / \|\nabla d\|$  denotes the velocity of the UAV in the opposite direction of the gradient of  $d$ ; and  $\gamma, \delta, \chi$  are functions of time. These parameters can also represent uncertainties of the system that will be specified later (see Remarks 4.2, 4.3).

**Theorem 4.1:** Consider the system (27). Choose  $k_P$  and  $k_D$  such that  $\gamma$ ,  $\delta$  and  $\chi$  are positive and bounded functions of time and define the following parameters:

$$\underline{d} = d^* \chi_{\min}$$

$$\bar{d} = d^* \chi_{\max}$$

and,

$$\mu^+ = \frac{k_P}{k_D} \frac{(\gamma\chi)_{\max}}{\delta_{\min}} v^*, \quad \bar{d} = \bar{d} \exp\left(\frac{m \|\nabla d\|_{\max} \mu^+}{k_D \delta_{\min}}\right) > \bar{d}$$

$$\mu^- = -\frac{k_P}{k_D} \omega^* \frac{\gamma_{\max}}{\delta_{\min}} \bar{d}, \quad \underline{d} = \underline{d} \exp\left(\frac{m \|\nabla d\|_{\max} \mu^-}{k_D \delta_{\min}}\right) < \underline{d}$$

Then, for all initial conditions such that  $d_0 > 0$ , the closed-loop trajectory exists for all time,  $d(t) > 0$  remains positive and  $(d, \dot{d})$  remain bounded. Moreover, the domain  $\mathcal{D}$  defined in Figure 4 represents the global attractor of the system; that is, it is forward invariant under dynamics (27) and for all bounded initial condition  $(d_0 > 0, v_d(0))$ , there exists a time  $t'$  such that  $(d, v_d) \in \mathcal{D}$  for all time  $t > t'$ .

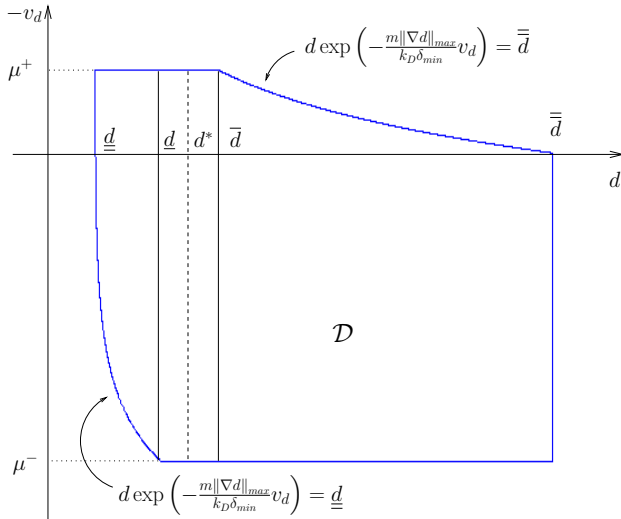


Fig. 4: Global attractor  $\mathcal{D}$

*Proof:* Define the following virtual state:

$$z = d \exp\left(\int_0^t -\frac{m \|\nabla d\| \dot{v}_d}{k_D \delta(\tau)} d\tau\right) \quad (28)$$

Differentiating  $z$  and recalling equations (27), it yields

$$\dot{z} = -\frac{k_P \omega^*}{k_D} \frac{\gamma(t) \|\nabla d\|}{\delta(t)} \left(1 - \frac{d^*}{d} \chi(t)\right) z \quad (29)$$

It is straightforward to show that if  $d > \bar{d}$ ,  $\dot{z} < 0$  and if  $d < \underline{d}$ ,  $\dot{z} > 0$ . Thus, four situations need to be considered:

$d_0 < \underline{d}$	$v_d(0) \leq 0, d \nearrow$	(a)
$z \nearrow$	$v_d(0) > 0, d \searrow$	(b)
$d_0 > \bar{d}$	$v_d(0) < 0, d \nearrow$	(c)
$z \searrow$	$v_d(0) \geq 0, d \searrow$	(d)

- 1) Case (a): since  $z$  is increasing, the sign of  $v_d$  (or  $\dot{d}$ ) cannot change as long as  $d \leq \underline{d}$ . Then there exists a time  $T$  such that  $d(T) \geq \underline{d}$ .
- 2) Case (d): since  $z$  is decreasing, there exists a time  $T$  such that  $d(T) \leq \bar{d}$ .
- 3) Case (b): to show that there exists a time  $T'$  such that the sign of  $v_d$  changes along with  $d(T') > 0$ , we proceed using a proof by contradiction. Assume  $v_d > 0$  and  $d < \underline{d}$  for all time  $t$ . Using the fact that  $\underline{d} = d^* \chi_{\min}$  it follows, from (28), that  $\dot{v}_d < 0$  while  $z$  remains positive and bounded

$$z < d_0 \exp\left(\frac{m \|\nabla d\|_{\max} v_d(0)}{k_D \delta_{\min}}\right)$$

for all time  $t$ . Note that  $\|\nabla d\|$  is bounded on all space. Moreover, since  $z$  is exponentially increasing, there exists  $\epsilon > 0$  such that  $\dot{z} > \epsilon z$ . Therefore, there exists a time  $t_1$  such that

$$z(t_1) > d_0 \exp\left(\frac{m \|\nabla d\|_{\max} v_d(0)}{k_D \delta_{\min}}\right)$$

This contradicts the assumption. Moreover, since  $z_0$  is positive,  $d$  remains positive. It follows that situation (b) leads to situation (a).

- 4) Case (c): analogously to the case (b) a similar proof shows that the situation (c) leads to situation (d). Consequently, for any situation (a-d), there exists a time  $T$  such that  $d(T)$  belongs to the interval  $(\underline{d}, \bar{d})$ .

To define the attractor, assume that  $(d_0 > 0, v_d(0)) \notin \mathcal{D}$ . Define the storage function  $\mathcal{J} = m(v_d)^2/2$ . Differentiating  $\mathcal{J}$  and recalling equations (27), it yields:

$$\dot{\mathcal{J}} = -k_D \delta \frac{v_d}{d} \left(v_d - \frac{k_P \omega^*}{k_D} \frac{\gamma}{\delta} (d - \chi d^*)\right) \quad (30)$$

$$= -k_D \delta \frac{v_d}{d} (v_d + \mu_{\gamma, \chi, \delta}(d)) \quad (31)$$

It follows that  $\mathcal{J}$  is negative as long as  $|v_d| > |\mu_{\gamma, \chi, \delta}(d)|$ . This implies that there exists a time  $T$  such that  $-v_d$  belongs to  $(\mu^-, \mu^+)$  for all time  $t \geq T$ . Combining this result with the previous discussion, we get the following table that represents the successive states of the system when the worst case occurs.

	phase 0	phase 1	phase 2	phase 3
(a)	$d_0 < \underline{d}$ $v_d(0) < -\mu^+$	$\underline{d} \leq d \leq \bar{d}$ $v_d < -\mu^+$	$\equiv$ (c) at phase 0	
(b)	$d_0 < \underline{d}$ $v_d(0) > -\mu^-$	$d < \underline{d}$ $v_d = 0$	$d < \underline{d}$ $0 > v_d > -\mu^+$	$d \in \mathcal{D}$
(c)	$d_0 > \bar{d}$ $v_d(0) < -\mu^+$	$d > \bar{d}$ $v_d = 0$	$\equiv$ (d) at phase 0	
(d)	$d_0 > \bar{d}$ $v_d(0) > -\mu^-$	$\underline{d} \leq d \leq \bar{d}$ $v_d > -\mu^-$	$\equiv$ (b) at phase 0	

A straightforward examination shows that for any initial condition, there exists a time  $T$  such that  $(d(T), v_d(T)) \in \mathcal{D}$ . It remains to show that if  $(d_0, v_d(0)) \in \mathcal{D}$ ,  $(d(t), v_d(t))$  remains in  $\mathcal{D}$  for all time  $t$ . Since, by assumption,  $v_d(0) \geq -\mu^+$ , this proves that  $v_d \geq -\mu^+$  for all time. Moreover,

since  $z$  is decreasing for  $d > \bar{d}$ , if the situation (c) occurs, then  $\dot{v}_d > 0$  and

$$d(t) \exp\left(-\frac{m \|\nabla d\|_{max}}{k_D \delta_{min}}(v_d - v_d(0))\right) \leq z(t) \leq z_0 = d_0$$

as long as  $v_d < 0$ . Thus,  $d \leq \bar{d}$  for all time. Using this result and the fact that  $v_d(0) \leq -\mu^-$  is also verified, it is straightforward to show, from equation (30), that  $v_d \leq -\mu^-$  for all time. Moreover, since  $z$  is increasing for  $d < \underline{d}$ , if the situation (b) occurs, then  $\dot{v}_d < 0$  and

$$d(t) \exp\left(-\frac{m \|\nabla d\|_{max}}{k_D \delta_{min}}(v_d - v_d(0))\right) \geq z(t) \geq z_0 = d_0$$

as long as  $v_d > 0$ . Thus,  $d(t) \geq \underline{d}$  for all time. Consequently,  $(d, v_d)$  remains in  $\mathcal{D}$  for all time. ■

*Remark 4.2:* If the optical flow is noisy. The noise can be modeled by a bounded variable  $b(t)$ ; that is:

$$w = \frac{v}{d} + b(t) \quad (32)$$

Let  $b_1$  be the component of  $b$  in the direction of the forward velocity  $v^{\parallel}$  and  $b_2$  the component of  $b$  in the direction  $\beta$ . Then, the dynamics of the system can be written as follows:

$$m\dot{v}_d = k_P \omega^* \gamma'(t) \left(1 - \frac{d^*}{d} \chi'(t)\right) - k_D \delta(t) \frac{v_d}{d} \quad (33)$$

where,

$$\begin{aligned} \gamma' &= \gamma - \frac{\gamma}{\omega^*} \left(b_1(t) + \frac{k_D}{k_P} b_2(t)\right) \\ \chi' &= \frac{\chi \gamma}{\gamma'} \end{aligned}$$

Then, choosing  $k_P$ ,  $k_D$  and  $\omega^*$  such that  $\gamma'(t)$  is positive and bounded for all time and recalling Theorem 4.1, for all initial conditions such that  $d_0 > 0$ , the closed-loop trajectory exists for all time,  $d(t) > 0$  remains positive and  $(d, \dot{d})$  remains bounded.  $\triangle$

*Remark 4.3:* if the norm of the forward velocity  $v^{\parallel}$  is not constant but under bounded and non-vanished ( $\|v^{\parallel}\| \geq v_{min} > 0$ ), the dynamics of the *pseudo distance*  $d$  can be written as follows:

$$m\dot{v}_d = k_P \omega^* \gamma(t) \left(1 - \frac{d^*}{d} \chi'(t)\right) - k_D \delta(t) \frac{v_d}{d} \quad (34)$$

where  $\chi'(t) = \chi \frac{\|w_{\beta}^{\parallel}\|}{\|w_{\beta}^{\parallel}\|_{v^{\parallel}=v^r}}$ . Recalling Theorem 4.1, it shows that the vehicle is ensured to follow the terrain without collision.  $\triangle$

## V. SIMULATIONS

In this section, simulations of the above algorithm designed for the full dynamics of the system are presented. Two cameras are incorporated in a 3-D simulator: one camera pointing down and the other one looking forward. The UAV is simulated with the model provided by Section II. A Pyramidal implementation of the Lucas-Kanade [19] algorithm is used to compute the optical flow. Control Law (14-15) is used for the terrain following. Results present the estimation of the slope  $\alpha$  computed from the measurement

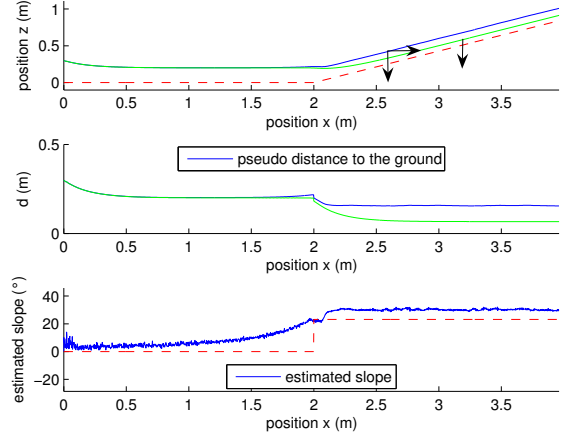


Fig. 5: Terrain following

of  $\beta$  (10) and the realised trajectory of the UAV. The profile of the terrain and its slope angle are represented by the red dashed lines in Figures 5 and 6 respectively. Figure 5 is the result related to the first example presented in Section III-B.1. The slope is set to 43%; it corresponds to  $\alpha = 23.3^\circ$ .  $v^*$  is set to  $0.05 \text{ m.s}^{-1}$  and  $\omega^*$  is set to  $0.25 \text{ s}^{-1}$ . This implies that  $d^* = 0.2 \text{ m}$ . The blue line is the result using both cameras while the green line represents the result when camera pointing down (see arrows on the figure) is used alone (see previous work [14]). Clearly, the use of two cameras improves performance, although the *pseudo distance* (result with two cameras) still does not converge to the desired one. This is due to arguments discussed in Section III-A, in particular the error due to not knowing  $M(\eta_0, \eta) \neq I_3$ .

Figures 6 and 7 provide results for the second situation described in Section III-B.2. It considers the problem of corner avoidance (typically the corner of a room). The result, in blue line, is performed when choosing  $k_P = 3k_D$  and using the same desired set points  $(v^*, \omega^*, d^*)$ . This shows good performance and a robust behaviour of the controller during transients.

## VI. EXPERIMENTAL RESULTS

In this section, experimental results of the above algorithm designed for the full height dynamic of the system are presented. The UAV used for the experimentation is the quadrotor, made by the CEA, (Fig. 8) which is a vertical take off and landing vehicle ideally suited for stationary and quasi stationary flight. The complete description of the prototype used is given in [20].

It is equipped with an Inertial Measurement Unit (IMU) and with two cameras (one camera pointing down and the other one looking forward). Each camera transmits video to a ground station (PC) via a wireless analogical link of 2.4GHz. The images sent by embedded cameras are received by the ground station at a frequency of 25Hz. In parallel, the X4-flyer sends the inertial data to the station on the ground at a

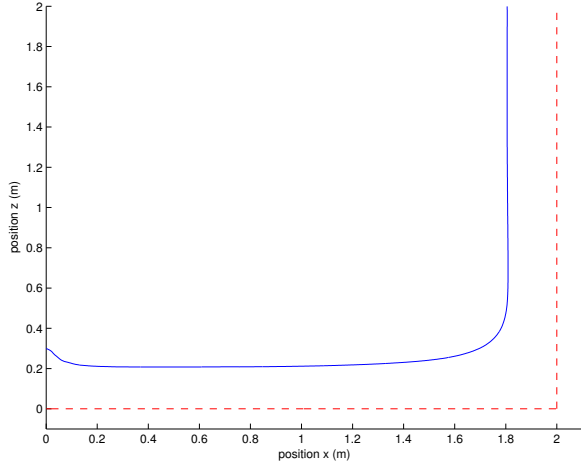


Fig. 6: Corner avoidance

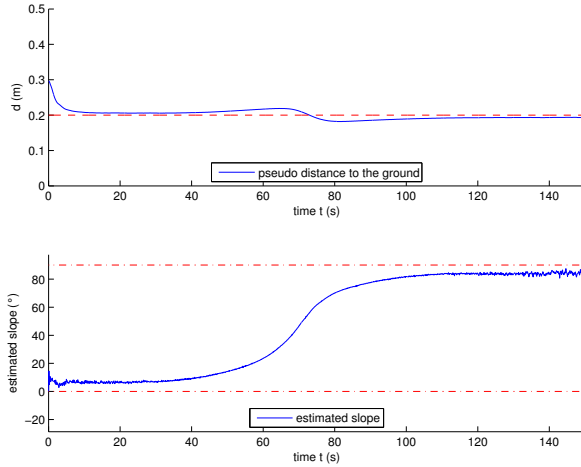


Fig. 7: Pseudo distance  $d$

frequency of 12Hz. The data is processed by the ground station PC and incorporated into the control algorithm. Desired orientation and desired thrust are generated on the ground station PC and sent to the drone. A key difficulty of the algorithm implementation lies in the relatively large time latency between the inertial data and visual features. For orientation dynamics, an embedded ‘high gain’ controller in the DSP running at 166Hz, independently ensures the exponential stability of the orientation towards the desired one.

### A. Experiments

Corner avoidance has been tested and results are presented. The task considered consists in avoiding frontal obstacle by going over it. The experiment is a direct application of the second example III-B.2. To regulate forward velocity to the desired set point, a controller based on the measure of the drag force opposite to the direction of motion via the combination of accelerometer readings and pressure measurement (barometer) is used. Note that this kind of

controller can be used only for indoor environment or very calm outdoor environment since the wind would disturb the measure of the velocity. In outdoor applications, this approach could be replaced by a velocity control based on GPS, an approach that is impossible in indoor environments. The lateral position has been stabilised with an optical flow based controller (see [21]). Textures are made of random contrasts (Fig. 8). A Pyramidal implementation of the Lucas-Kanade [19] algorithm is used to compute the optical flow. The sample time of 12Hz and large time latencies prevent us from experimenting algorithms with high velocities of the quadrotor. Then  $v^*$  is set to  $0.4 \text{ m}\cdot\text{s}^{-1}$ . Moreover,  $\omega^*$  is set to  $0.5 \text{ s}^{-1}$  and therefore  $d^* = 0.8 \text{ m}$ . The parameters  $k_P$



Fig. 8: Hovering flight around the textured terrain

and  $k_D$  have been chosen such that the variable  $\chi$  defined in Section III-B.2 is positive:

$$k_P > 0.36k_D \quad (35)$$

During experiments, the yaw velocity is not controlled. The drone is teleoperated near the target, so that textures are visible. Figure 9 shows the measurement of the forward velocity  $v^{\parallel}$ , the measurement of the forward optical flow  $w_{\beta}^{\parallel}$  and the measurement of the pseudo distance  $d = \|v^{\parallel}\| / \|w_{\beta}^{\parallel}\|$ . The result shows that  $v^{\parallel} \rightarrow v^*$  and  $w_{\beta}^{\parallel} \rightarrow \omega^*$ . Several experiments have been carried out to verify the performance of the approach. One can see that it ensures that the quadrotor follows the terrain without collision. This result can be watched on the video accompanying the paper. Figure 10 shows the same results in the case of a more complex terrain made of a corner followed by an elevated level and a ramp that slopes down. This result can also be watched on the same video accompanying the paper.

## VII. CONCLUDING REMARKS

This paper presented a rigorous nonlinear controller for terrain following of a UAV using the measurement of average optical flow in multiple observation points. The approach is

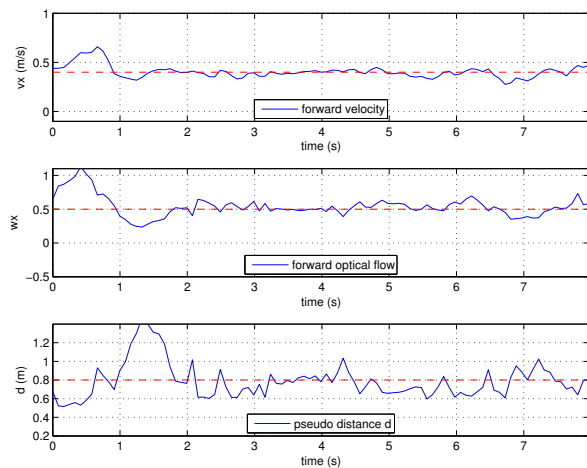


Fig. 9: Corner avoidance

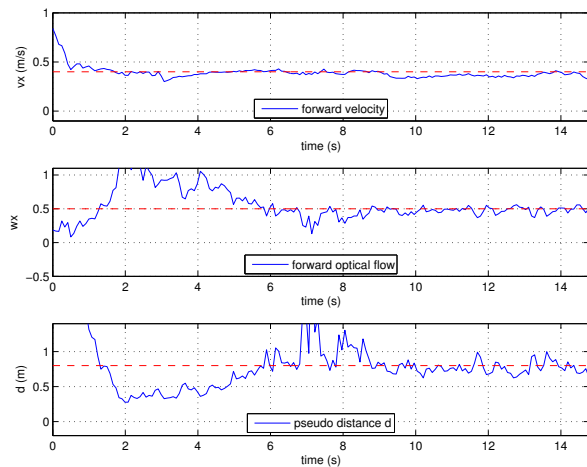


Fig. 10: Terrain following with corner avoidance

a generalization of a prior work that used only one direction of observation. The closed-loop system and limits of the controller have been theoretically analysed and discussed. The proposed control algorithm has been tested in simulation in different scenarios and then implemented on a quad-rotor UAV to demonstrate the performance of the closed loop system. Although only a longitudinal motion was considered, the approach can be extended to full 3-D motion by adding additional cameras.

## VIII. ACKNOWLEDGMENTS

This work was partially funded by Naviflow grant and by ANR project SCUAV (ANR-06-ROBO-0007) and by the Australian Research Council through the ARC Discovery Project DP0880509, "Image based teleoperation of semi-autonomous robotic vehicles".

## REFERENCES

- [1] K. P. Valavanis, *Advances in Unmanned Aerial Vehicles*. Springer, 2007.
- [2] J. Koenderink and A. van Doorn, "Facts on optic flow," *Biol. Cybern.*, vol. 56, pp. 247–254, 1987.
- [3] M. Srinivasan, S. Zhang, J. S. Chahl, E. Barth, and S. Venkatesh, "How honeybees make grazing landings on flat surfaces," *Biological Cybernetics*, vol. 83, p. 171183, 2000.
- [4] G. L. Barrows, J. S. Chahl, and M. V. Srinivasan, "Biomimetic visual sensing and flight control," in *Seventeenth International Unmanned Air Vehicle Systems Conference*, Bristol, UK, April 2002.
- [5] F. Ruffier and N. Franceschini, "Visually guided micro-aerial vehicle: automatic take off, terrain following, landing and wind reaction," in *Proceedings of international conference on robotics and automation*, LA, New Orleans, April 2004.
- [6] W. E. Green and P. Y. Oh, "Optic flow based collision avoidance," *IEEE Robotics & Automation Magazine*, vol. 15(1), pp. 96–103, 2008.
- [7] J. S. Humbert, R. M. Murray, and M. H. Dickinson, "Pitch-altitude control and terrain following based on bio-inspired visuomotor convergence," in *AIAA Conference on Guidance, Navigation and Control*, San Francisco, CA, 2005.
- [8] F. Ruffier and N. Franceschini, "Optic flow regulation: the key to aircraft automatic guidance," *Robotics and Autonomous Systems*, vol. 50, pp. 177–194, 2005.
- [9] M. A. Garratt and J. S. Chahl, "Vision-based terrain following for an unmanned rotorcraft," *Journal of Field Robotics*, vol. 25, pp. 284–301, 2008.
- [10] L. Muratet, S. Doncieux, Y. Briere, and J.-A. Meyer, "A contribution to vision-based autonomous helicopter flight in urban environments," *Robotics and Autonomous Systems*, vol. 50, no. 4, pp. 195–209, 2005.
- [11] A. Beyeler, J.-C. Zufferey, and D. Floreano, "Vision-based control of near-obstacle flight," *Autonomous Robots*, vol. 27, no. 3, pp. 201–219, 2009. [Online]. Available: <http://www.springerlink.com/content/4654127632552734/>
- [12] J. Serres, D. Dray, F. Ruffier, and N. Franceschini, "A vision-based autopilot for a miniature air vehicle: joint speed control and lateral obstacle avoidance," *Autonomous Robots, Springer*, vol. 25, no. 1-2, pp. 103–122, August 2008.
- [13] F. Ruffier and N. Franceschini, "Aerial robot piloted in steep relief by optic flow sensors," in *IEEE/RSJ Int. Conf. on Intelligent Robots and Systems*, Nice, France, September 2008, pp. 1266–1273.
- [14] B. Herisse, T. Hamel, R. Mahony, and F.-X. Russotto, "A nonlinear terrain-following controller for a vtol unmanned aerial vehicle using translational optical flow," in *IEEE Int. Conf. on Robotics and Automation*, Kobe, Japan, May 2009.
- [15] S. Bertrand, T. Hamel, and H. Piet-Lahanier, "Stability analysis of an uav controller using singular perturbation theory," in *Proceedings of the 17th IFAC World Congress*, Seoul, Korea, July 2008.
- [16] R. Mahony and T. Hamel, "Robust trajectory tracking for a scale model autonomous helicopter," *International Journal of Non-linear and Robust Control*, vol. 14, pp. 1035–1059, 2004.
- [17] J. L. Barron, D. J. Fleet, and S. S. Beauchemin, "Performance of optical flow techniques," *International Journal of Computer Vision*, vol. 12, no. 1, pp. 43–77, 1994.
- [18] H. K. Khalil, *Nonlinear Systems*, 2nd ed. New Jersey, U.S.A.: Prentice Hall, 1996.
- [19] B. Lucas and T. Kanade, "An iterative image registration technique with an application to stereo vision," in *Proceedings of the Seventh International Joint Conference on Artificial Intelligence*, Vancouver, 1981, pp. 674–679.
- [20] N. Guenard, T. Hamel, and R. Mahony, "A practical visual servo control for an unmanned aerial vehicle," *IEEE Transactions on Robotics*, vol. 24, pp. 331–340, 2008.
- [21] B. Herisse, F.-X. Russotto, T. Hamel, and R. Mahony, "Hovering flight and vertical landing control of a vtol unmanned aerial vehicle using optical flow," in *IEEE/RSJ Int. Conf. on Intelligent Robots and Systems*, Nice, France, September 2008.